JOURNAL OF PROPULSION AND POWER
Vol. 27, No. 3, May–June 2011

Experimental Investigations of the Performance of a Multitube Pulse Detonation Turbine System

Adam Rasheed,* Anthony H. Furman,† and Anthony J. Dean‡
General Electric Global Research, Niskayuna, New York 12309

DOI: 10.2514/1.B34013

A multitube pulse detonation combustor consisting of eight unvalved tubes arranged in a can-annular configuration was integrated with a single-stage axial turbine nominally rated for 10 lbm/s, 25,000 rpm and 1000 hp. The multitube pulse-detonation-combustor-turbine hybrid was operated using ethylene-air mixtures for runs of 5 + min to achieve thermal steady state in order to quantify performance at two operating conditions using simultaneous and sequential firing patterns. Analysis of these data reveal that turbine efficiency under pulse-detonation-combustor-fired operation was indistinguishable from steady performance within the ±8 points measurement uncertainty. Furthermore, the pulse-detonation-combustor-turbine hybrid system demonstrated a potential 25% improvement in efficiency once corrections were made for the suboptimal fueling design, which resulted in lower-than-anticipated combustion efficiency. The present work is promising as it suggests that a pulse-detonation-combustor-turbine hybrid engine performance benefit can be realized with further development.

Nomenclature

C_p	=	specific heat at constant pressure
h	=	enthalpy
m	=	mass flow rate
P	=	pressure
T	=	temperature
Q	=	heat input
W	=	power
γ	=	ratio of specific heats

Subscripts

c	=	compressor
t	=	turbine
$1c$	=	compressor inlet
$2c$	=	compressor exit
3	=	pulse-detonation-combustor inlet (compressor discharge)
4	=	turbine inlet
5	=	turbine exit

I. Introduction

PULSE detonation engines (PDEs) have been proposed for aerospace propulsion for more than 50 years [1] and have been considered for potential applications across the flight envelope spanning subsonic, supersonic and hypersonic flight [2–4]. These engines rely on pressure-rise detonation, which is a supersonic shock-induced combustion wave [5], rather than constant pressure deflagration currently used in aerospace propulsion engines. For a Chapman–Jouguet detonation, the incident shock wave and trailing combustion zone are coupled such that the temperature rise across the shock initiates the combustion whose subsequent heat release provides energy to sustain the shock. Many of the proposed propulsion applications rely directly on the impulse thrust of the detonation in a simple pure tube PDE configuration where the detonation exhausts directly into the ambient atmosphere. Advanced concepts have also been proposed such as hybrid-PDE gas-turbine engine configurations where the standard steady-flow deflagration combustor is replaced with multiple pulse detonation combustors (PDCs) as shown notionally in Fig. 1. PDEs have drawn attention because of their potential for increased specific impulse when compared with ramjets [6–9]. Furthermore, notional thermodynamic cycles show increased thermodynamic efficiency greater than Humphrey (constant volume) and Brayton (constant pressure) cycles as a result of the pressure-rise associated with a detonation [10–12].

Recently, there have been significant advances in the development of PDE technology. In particular, numerical and experimental investigations have focused on the importance of a converging-diverging exit nozzle to optimize the specific impulse [13–15], thrust augmentation using ejectors [16–18], detonation of liquid fuels [19–21], effect of ambient pressure on specific impulse [22] and nonintrusive laser-based time-resolved instrumentation [23,24]. Additional work has focused on experimental demonstrations of multitube PDEs [25,26] and PDC-turbine hybrid configurations as summarized in Rasheed et al. [27].

The present paper examines the performance of the PDC-turbine hybrid concept. Although specific concepts vary in their implementation, a common feature incorporates the idea of the combustion products from the pulse detonation chambers driving a downstream turbine. Numerical studies using the numerical propulsion systems simulation incorporated pulse detonation combustors into the core of a commercial turbofan producing 2% higher thrust and 8 to 10% lower specific fuel consumption than the baseline engine [28]. Further studies using cycle-deck analysis and quasi-one-dimensional codes for ground-based power generation applications showed potential improvements in thermal efficiency of almost 20% compared with conventional gas-turbine technology [29,30]. These investigations considered both simple cycle and combined cycle configurations. The potential for step-changes in gas-turbine engine performance has attracted a strong interest internationally with significant efforts underway in Japan [31] and China [32], where studies are showing similar large performance benefits. The first experimental studies of PDC-turbine hybrid performance were reported by Hoke et al. [33] and Schauer et al. [34], in which a PDE supplying an automotive-based centrifugal turbine coupled to a centrifugal compressor was studied. Turbine performance was measured by regulating compressor outlet pressure, measuring inlet flow, and determination of operating conditions. The turbine was spun to over 130,000 rpm, and was studied over the majority of the operating map. At selected operating points, comparisons to

Received 12 May 2010; revision received 24 October 2010; accepted for publication 25 October 2010.

*Aerospace Research Engineer. Associate Fellow AIAA.
†Turbomachinery Research Engineer.
‡Manager, Propulsion Systems Laboratory. Member AIAA.

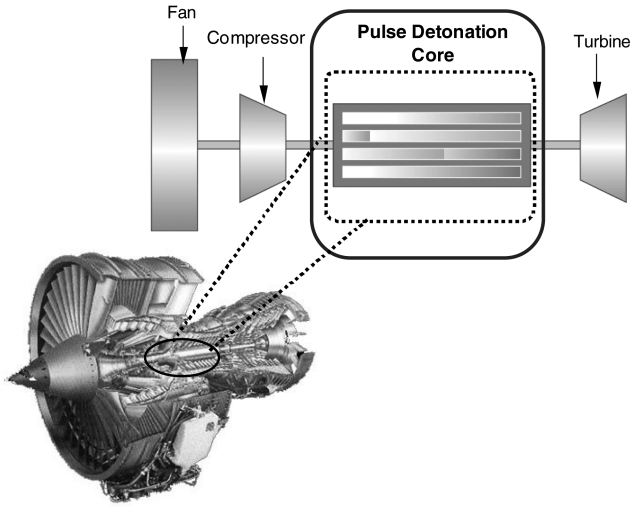

Fig. 1 PDC-turbine hybrid engine concept.

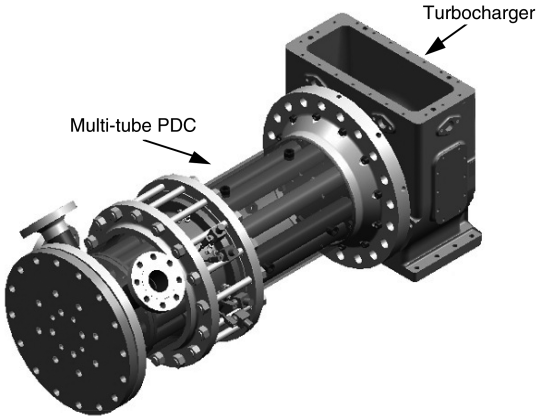

Fig. 2 Solid model of the PDC-turbine hybrid system used for the present experiments.

theoretical calculations revealed high losses during work extraction by this nonoptimized turbine. Another study used a single tube impulse turbine (Elliott PYR model partial admission steam turbine) rig with a rating of 1 lbm/s, 5000 rpm and 100 hp. The rig was fired for 3 min and generated 20 hp with a turbine inlet temperature of 800°F [35]. No estimates for the efficiency were provided. Recently, a small-scale multitube PDC-turbine hybrid has been tested consisting of an annular array of six 25.4 mm (1 in). tubes detonating stoichiometric $C_2H_4 - O_2$ into a 6.1″ diameter single-stage axial turbine (JFS-100-13A) with nominal rating of 1.6 lbm/s, 60,400 rpm and 90 hp. PDC-fired operation was performed to thermal steady state (approximately 90 s for this rig) at pressure ratios between 1.01 and 1.45 showing that the normalized power was sensitive to fill fraction and equivalence ratio [36–38], however, the results seemed confounded with the presence of a gearbox on the shaft outtake. The most recent work used a novel optical technique using a laser pointer and a photodiode to characterize the pulse-to-pulse change in turbine rpm [39]. By sampling at high-frequency, the effect of the individual detonation pulses could be seen as a "stair-stepping" increase in speed during the turbine spin-up. As highlighted by these studies, one of the main challenges in developing a PDC-turbine hybrid is to assess the effect of periodic, high-pressure pulses (decaying blast waves) on turbine performance and to quantify the benefit to overall cycle efficiency.

The present paper describes experiments investigating a large-scale multitube PDC-turbine hybrid device representative of a potential aircraft propulsion system. These experiments were performed as part of the pulse detonation engine turbine interaction program (PDE TIP) [27]. The multitube PDC-turbine hybrid system consisted of eight unvalved tubes arranged in a can-annular configuration integrated with a single-stage axial turbine nominally rated for 10 lbm/s, 25,000 rpm and 1000 hp. The system accumulated 145 min of operation including many runs of 5+ min for the rig to achieve thermal steady state (as measured by the turbine stator metal temperature and the turbine inlet gas temperature) and for the turbine to attain constant speed. The rig was operated at frequencies up to 30 Hz (per tube) in different firing patterns using stoichiometric C_2H_4-air mixtures at conditions up to 8 lbm/s, 22,000 rpm and 750 hp. A comprehensive dataset was obtained investigating operability, noise, performance, and mechanical response [27,40]. The focus of the present paper is to quantify the turbine performance and overall efficiency of this system.

II. Experimental Setup

A. PDC-Turbine Hybrid System

For the present investigations, a PDC-turbine hybrid system was designed and built by integrating a multitube PDC system with a single-stage axial flow turbine. Figure 2 shows a solid model of the experimental rig. The multitube PDC consisted of eight unvalved PDCs arranged in a can-annular configuration on a 292 mm (11.5 in.) circle to line-up as closely as possible with the midspan of the turbine blades [which was on a 305 mm (12 in.) circle]. The 6 mm (0.25 in.) offset between the tube centerline and blade midspan was required for the tubes to fit into the standard 16″ pressure vessel used for the outer case. The multitube PDC had an overall length of 1.5 m (5 ft), The downstream flange was designed to mate to either the turbine casing (turbocharger) or a standard 16″ 300 lb flange so that the rig could also be tested by firing into a backpressured 16″ pressure vessel rig (i.e., without turbomachinery downstream).

A cross section of the experimental apparatus is shown in Fig. 3. Each tube was 49.3 mm (1.939 in.) in diameter (2″ schedule 80 pipe) with a length of 800.1 mm (31.5 in.) as measured from the downstream face of the fuel-air mixing element to the tube exit. This length was selected since it represented the distance in which C_2H_4-air detonation could be achieved using the implemented technology. A spark plug was mounted approximately one diameter downstream of the fuel-air mixing element to allow a short distance for the fuel and air to mix prior to ignition. A water-cooled spiral deflagration-to-detonation transition (DDT) geometry was used to assist the detonation process. Air was continuously flowed through the system (*i.e.*, no valve on the air side), while the fuel injection was pulsed using two high-frequency valves mounted in parallel on each tube. Note that an orifice plate was used to choke the flow at the inlet to the primary plenum in order to isolate the facility piping from the rig. Each individual tube, however, was unchoked relative to the primary plenum. The effective area of each fuel valve had been independently determined experimentally and they were deliberately paired so that each PDC tube had the same net effective area across the fuel valves. High-speed shadowgraph imagery was used to verify that each of the

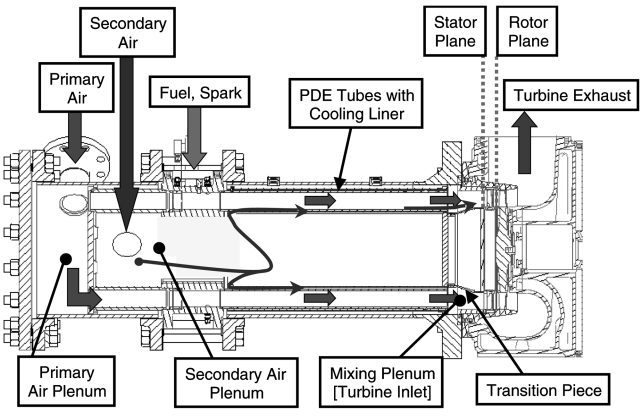

Fig. 3 Cross section of the PDC-turbine hybrid system.

valves had an open and close time of 2 and 5 ms, respectively. Each PDC was shrouded with a coaxial liner for secondary flow to provide backside cooling of the PDCs. This configuration for each PDC tube was chosen because of the extensive prior experience with similar configurations [22]. A rigorous risk reduction test program was conducted on a single tube implementation of the exact configuration prior to testing the multitube PDC.

The individual PDCs shared a common primary air-inlet, as well as a common exit (in the transition region to allow for mixing) prior to entering the turbine. The primary air was supplied by facility compressors in a "direct-connect" test arrangement. The secondary flow (bypass) air was ducted through coaxial cooling liners around each PDE tube for thermal management and then mixed with the primary detonated air in the transition region prior to entry into the turbine. Increasing the amount of cold secondary flow maintained the average temperature within the turbomachinery material temperature limits without changing the primary flow (and having to readjust the fuel fill and spark timing for the PDC). The secondary flow air was also provided by facility compressors on a separate air line with independent control from the primary air flow. The transition piece consisted of a tapered truncated cone that matched the inner diameter (ID) from the PDE exit plane to the larger ID of the turbine inlet plane. The distance from the PDE exit to the stator inlet (*i.e.*, the axial length of the transition piece) was 10.7 mm (4.2 in.). The 356 mm (14 in.) diameter single-stage axial turbine (one stator and one rotor) was from a locomotive scale turbocharger designed for nominal flows of 10 lbm/s, 25,000 rpm and 1000 hp. The compressor side of the turbocharger was on a separate air-loop (drawing air from the ambient test cell) and used as the load for the turbine operation.

Throughout the design and manufacture, significant effort was made to ensure that each tube was geometrically identical and, whenever possible, an appropriate tuning knob was included in the design. This was deemed to be critical in order to minimize tube-to-tube variations during fired operations. For example, each PDC had an inlet flow adjustor that consisted of two slotted plates that could be rotated relative to one another to either decrease or increase the flow area to each tube. In this manner, each tube could be individually adjusted to have the same air flow rate. As described previously, the fuel valves were paired to match the effective areas to minimize any variation in fuel mass flow rate from tube-to-tube. In addition, the fuel valve manifold to the rig was specifically designed so that each tube had the same length of tubing from the common fuel manifold and each leg had a quarter-turn valve that could be used to adjust the fuel flow to each individual tube. The overall rig was designed for simplicity, ease of manufacturing and assembly, modularity for modifications, multiple access ports for instrumentation and minimization of tube-to-tube variations.

B. Instrumentation

The PDC-turbine hybrid system was fully instrumented with mass flow measurements, flowpath temperatures and static pressures, surface thermocouples, an optical pyrometer, accelerometers, proximity probes for rotor dynamics, strain gauges and an optical blade tip deflection measurement system. For short duration ($\sim$1 s) firings, high-frequency piezoelectric static pressure sensors (PCB P113A) distributed throughout the rig were used to capture the wave dynamics, however, for long duration firings, they were removed since the sensors were temperature limited. For the present investigation, the turbine inlet and exit temperatures were measured using an array of 1/8″ Type K shielded thermocouples that were located 56 mm (2.2 in.) upstream of the stator leading edge (F-plane) and 25 mm (1 in.) downstream of the PDC exit (*Z*-plane). These thermocouples penetrated into the flowfield such that they were approximately at the midspan position of the blades. For the first entry into the test cell, three such thermocouples were used as shown in Fig. 4a. The schematic clearly shows the location of the thermocouples, whereas the photograph requires a bit more effort to see the thermocouples penetrating into the flowfield. One of the thermocouples was directly in-line with PDC tube 6 (F135), while the other two thermocouples were between PDC tubes 6 and 7

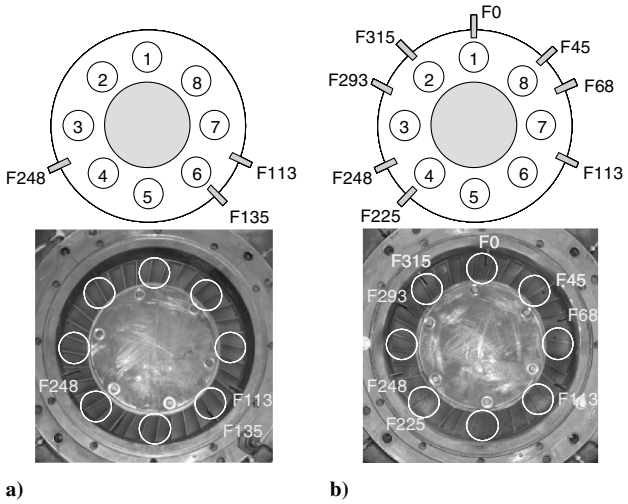

a) b)

Fig. 4 Turbine inlet temperature instrumentation for a) test entry 1 and b) test entry 2.

(F113), and PDC tubes 3 and 4 (F248), respectively. For the second entry into the test cell, more thermocouples were added in order to decrease the uncertainty and better understand the pattern factor as shown in Fig. 4b. A total of eight thermocouples were used, four of which were directly in-line with PDCs (F0, F45, F225, and F315), while the remaining four were between PDCs (F68, F113, F248, and F293).

To measure detonation wave velocities, each tube was instrumented with two custom built, low-profile, high temperature ion probes located at 660 mm (26 in.) and 760 mm (30 in.) from the fuel-air mixer. The ion probe signals were measured at high-frequency (1 MHz) in 1 s bursts, processed in real-time to calculate the detonation wave velocities and the summary statistics were recorded at 1 Hz for the duration of the run. The ion probes verified that the CJ velocity of approximately 1850 m/s was achieved for each run condition. Additionally, an emissions sample probe was located approximately 2 m downstream in the exhaust duct to measure O_2, CO_2 and unburned hydrocarbon (UHC) concentrations.

C. Data Acquisition Systems

Four data acquisition (DAQ) systems were used to monitor the rig during its operation: a low-speed DAQ ($\sim$1 Hz), a medium-speed DAQ ($\sim$24 kHz), a high-speed DAQ (1 MHz), and the rotor shaft vibration monitoring DAQ. The low-speed DAQ consisted of two Yokagawa MX-100 with eight MX-110-UNV-M10 universal modules for a total of 80 channels. The data were monitored and collected using an in-house DAQ software. This was the primary means of monitoring the rig during operation and recorded all flowpath temperatures and pressures, mass flow rates and metal temperatures. The medium-speed DAQ consisted of a Teac LX-10 data recording system with a sample rate of either 24 or 48 kHz per channel. This system was used to record the strain gauge signals using Encore M610-002 strain gauge amplifier modules. The high-speed DAQ consisted of three separate desktop systems using National Instruments hardware. Each desktop had the capability of sampling eight channels at 1 MHz per channel and was configured with two PCI-6110 synchronized DAQ boards. The high-speed DAQ was used to record the ion probe and PCB pressure transducer signals. The software was developed in-house with the particular feature of performing real-time processing of the ion probe signals into wave velocities that were then communicated and recorded on the low-speed DAQ.

D. Control Systems

The PDC-turbine hybrid rig consisted of two independent control systems monitored by an operator. The Honeywell Test Cell Facility Control System was used to set the primary and secondary air flows

Table 1 Experimental run conditions

Run	Power, kW	Turbine speed, rpm	Turbo steady baseline	PDE TIP steady	PDE TIP burner	PDE TIP fired
Condition A	75	12,000	——	——	——	——
Condition B	150	15,600	——	——	——	——

and also provided the necessary turbine overspeed protections and automated emergency stop functions. The Multitube PDC Control System (MTPCS) developed in-house was used to set the timing for the spark and fuel valves for each PDC tube, the firing frequency and the overall firing pattern. Once these parameters were set, the control system could be triggered to fire the multitube PDC for a desired duration. The MTPCS could operate the rig in excess of 40 Hz per tube, although for the present investigations, the firing frequency (per tube) was limited to 20 Hz. In addition to being able to fire any single tube individually, the MTPCS allowed the flexibility of firing the PDCs in any desired order. For the present experiments, the tubes were fired either simultaneously or sequentially.

III. Experimental Plan and Results

The PDC-turbine hybrid rig experiments were performed in two three-month test cell entries approximately 12 months apart. Long duration experiments were performed to quantify the performance under PDC-fired operation relative to steady-flow operation. Table 1 summarizes the two power conditions and the different operation modes for which data was collected. The performance data was obtained at 75 kW (100 hp) and 150 kW (200 hp) conditions under normal turbocharger steady-flow operation (nonvitiated), PDE TIP steady-flow operation (nonvitiated), PDE TIP steady-burner operation (vitiated) and PDC-fired operation (vitiated). Note that PDE TIP burner data was not obtained for Condition A since the steady burner would flameout at this low power condition. For the nonvitiated performance data, the facility compressors provided the desired air flow that passed through a heat-exchanger to achieve the desired rig inlet temperature.

The turbocharger steady-flow operation consisted of testing the turbine using the standard test cell piping and the production diffuser inlet duct for the turbocharger in its native installed configuration, whereas the PDE TIP steady-flow operation consisted of flowing steady, heated air through the PDE TIP rig (eg. 8-tube can-annular arrangement) installed with its own specific inlet piping. Both sets of data were collected to make sure there was no difference in turbine performance with the PDE TIP hardware installed. The performance data measurement techniques and analysis methods were validated by comparing the steady-flow data with baseline results from the production hardware.

For the steady-burner and PDC-fired operation, typical rig operation consisted of establishing a desired prefired steady-state condition using the primary and secondary air flows (i.e., air flowing continuously through the rig without combustion). Once the turbine speed stabilized and it was determined that all pressures and temperatures were nominal, the multitube PDC (or steady burners) were then fired for 5+ min to allow the turbine to spool-up to its new fired steady-state condition for performance measurements. The turbine would typically spool-up to near constant speed within 30 s, however, performance measurements were only taken after 4 to 5 min when the rig reached thermal steady state by averaging over a 30 s window. The term thermal steady state is used here to describe the condition where the hardware has reached a "heat-soak" condition as determined by monitoring surface mounted thermocouples (eg. the metal surface temperature has heated to a constant temperature and is no longer changing). PDC-fired operation was achieved using nominally stoichiometric 100% fill of C_2H_4-air mixtures. The firing frequency was set at 20 Hz (per tube) and two different firing patterns (simultaneous and sequential) were tested at both Condition A and B. The simultaneous firing pattern consisted of firing all tubes at the same time at 20 Hz. The sequential pattern fired each tube individually at 20 Hz in sequence phased lagged by 0.125 s.

IV. Performance Results

The present experiments quantified the performance of the PDC-turbine hybrid system both in terms of turbine component efficiency and overall rig efficiency. Although turbine component efficiency is important, the more relevant metric is the thermal efficiency of the engine (the specific fuel consumption or overall efficiency). For practical applications, it is possible that, for a PDC-turbine hybrid engine, the turbine component efficiency may be lower as compared with similar steady-flow gas-turbine engines. The overall engine efficiency, however, can still be higher if the benefits of the detonation combustion outweigh any unsteady losses. In particular, for the present experiments, the turbine was a standard turbomachinery design optimized for steady and spatially uniform flow. As such, it was expected that the turbine would exhibit degraded component efficiency under PDC-fired operation (relative to a steady flow).

A. Turbine Efficiency Analysis Method

The present approach was to validate the measurement technique by baselining the turbine performance under steady-flow (nonvitiated) with prior turbine maps. The results were then extended to steady-burner operation (vitiated) to confirm turbine performance under steady combustion before final comparisons were made with PDC-fired operation. The turbine performance was quantified in terms of the normalized power ($\Delta h/T$, where Δh is enthalpy change across the turbine and T is the turbine inlet temperature) and the turbine efficiency. Figure 5 shows a notional schematic of the present PDC-turbine hybrid experimental rig that defines the overall configuration and the relevant thermodynamic stations. The turbine power and efficiency were calculated by noting that the power generated by the turbine must equal the power required by the compressor (plus bearing losses) since they were on the same shaft. This "indirect method" minimized the uncertainty since it reduced the dependence on the turbine inlet temperature (T_4) and the turbine inlet gas properties (C_p and γ), both of which was found to be the largest contributors to the uncertainty.

The indirect turbine power was calculated as

$$\dot{W}_{t_{\text{indirect}}} = \dot{W}_c + \dot{Q}_{\text{Bearing Losses}} \tag{1}$$

where W_c is the compressor power calculated as

$$\dot{W}_c = \dot{m}(h_{2c} - h_{1c}) = \dot{m} C_p T_{1c}\left[\left(\frac{T_{2c}}{T_{1c}}\right) - 1\right] \tag{2}$$

and $Q_{\text{BearingLosses}}$ was estimated from the temperature rise in the bearing lubrication oil using

$$\dot{Q}_{\text{Bearing Losses}} = \dot{m}_{\text{Oil}} C_{p\text{Oil}} \Delta T_{\text{Oil}} \tag{3}$$

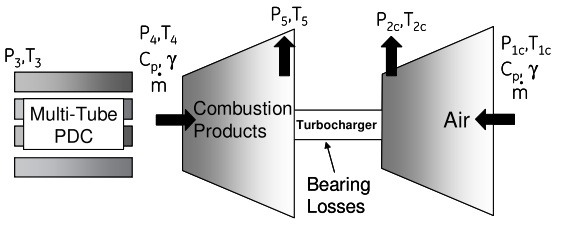

Fig. 5 Notional schematic of the PDC-turbine hybrid rig for performance measurements.

Table 2 Estimated uncertainties for the present performance measurements

Calculated value	Uncertainty
Power	±10%
Normalized power	±0.004
Turbine efficiency	±8 points
Pressure ratio	±0.05

where m_{Oil} is the mass flow rate of oil, $C_{p\text{Oil}}$ is the oil specific heat and ΔT_{Oil} is the measured temperature rise in the bearing oil. The turbine efficiency could then be calculated using

$$\eta_{t_{\text{indirect}}} = \frac{h_4 - h_5}{h_4 - h_{5s}} = \frac{\dot{W}_{t_{\text{indirect}}}}{\dot{m} C_{p\text{Turbine Inlet}} T_4 [1 - (\frac{P_5}{P_4})^{\frac{\gamma-1}{\gamma}}]} \tag{4}$$

A propagation of uncertainty analysis of the preceding equations showed that the turbine inlet temperature had a strong effect on the uncertainty of the turbine performance. Equation (1) shows the advantage of the indirect method since the turbine power does not require any knowledge of the turbine inlet conditions. Equation (4) shows that the turbine efficiency, however, still requires the turbine inlet temperature, which was measured to within ±50°F and was determined six different ways. The gas properties at the turbine inlet (*i.e.*, C_p and γ) were estimated by calculating the equilibrium combustor exit gas temperature of lean premixed ethylene-air reactant mixtures using different equivalence ratios until the computed temperature matched the measured turbine inlet temperature. This approach effectively provides gas properties that are mass-averaged for all the working fluid passing through the turbine. Table 2 summarizes the uncertainties determined using propagation of uncertainty analysis for the computed quantities.

A significant effort involved carefully quantifying the turbine inlet temperature because of its importance to the contribution of the overall performance measurements. The turbine inlet temperature was quantified six different ways: 1) measured turbine inlet temperature, 2) measured stator blade temperature, 3) combustor exit gas temperature based on O_2 concentration, 4) combustor exit gas temperature based on CO_2 concentration, 5) temperature estimated from power and measured downstream thermocouples, and 6) combustor exit gas temperature based on equivalence ratio (based on measured air and fuel mass flow rates) corrected for UHCs.

1. Measured Turbine Inlet Temperature

As described earlier, the turbine inlet temperature was measured using an array of type K thermocouples at the turbine inlet plane. The details of the thermocouples are provided in the Instrumentation section of the present paper. The uncertainty from this measurement was estimated by measuring the variation in the temperature measurements with nonvitiated steady flow. Figure 6 shows a time trace of the measured temperatures when the primary air (at 760°F) mass flow was increased from 3.5 to 4.0 lbm/s while decreasing the secondary air (at 90°F) from 1.5 to 1.0 lbm/s such that the total air mass flow through the turbine remained unchanged. The measured temperatures are clearly separated in two groups. The hotter group represents thermocouples directly in-line with PDCs and the colder group represents the thermocouples between PDCs with the straight-average of the thermocouples superimposed. The straight-average measurement is initially 530°F and rises to 590°F as the mass flows were adjusted. This can be compared with the calculated mass-weighted average temperature assuming full mixing (not shown on graph), which was calculated to be initially 560°F rising to 620°F. The estimated uncertainty of ±50°F for the turbine inlet temperature (T_4) comes from this figure. This temperature trace was typical of the steady-burner and PDC-fired operation as well.

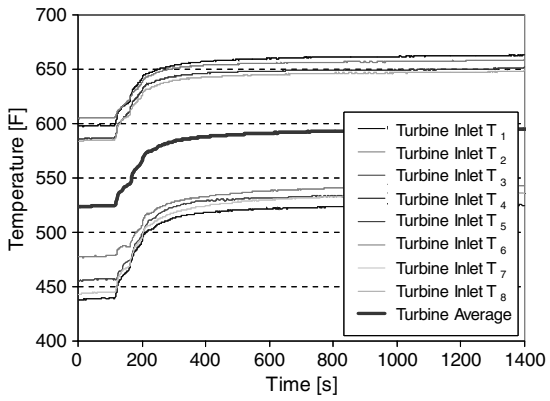

Fig. 6 Turbine inlet temperature traces showing pattern factor during PDE TIP steady flow.

2. Measured Stator Blade Temperature

The stator blade temperature was measured by imbedding 1 mm (0.040 in.) Type K thermocouples within the stator blades directly in-line with each PDC tube. Since the blades were uncooled it was reasonable to assume that, once thermal steady state was achieved, the stator blade metal temperature as measured by the imbedded thermocouples was approximately at the same temperature as the gas flow and represented an accurate measurement of the gas temperature.

3. Combustor Exit Gas Temperature Based on O_2 Concentration

For the second test entry, an emissions probe measured samples of the exhaust stream just prior to entering the exhaust tunnel. The exhaust ducting was insulated to help minimize any heat losses and the location of the probe was far enough downstream to insure adequate mixing of the flow. The O_2 concentration was measured using a California Analytical Model 100P analyzer that has been calibrated and was normally used for emissions measurements at the GEGR combustion test cells. The combustor exit gas temperature could then be estimated using an equilibrium calculation based on the measured O_2 concentration.

It should be noted that present-day emissions instrumentation used for steady-flow combustors have slow response times and cannot resolve the short time scales of the PDC cycle. Furthermore, the sample probes used today are not designed to ingest the PDC exit flow consisting of a detonation wave followed by widely varying flows. For these reasons, characterizing the emissions directly downstream at the exit of a PDC is very difficult. For the present work, the emissions probe was located as far downstream from the turbine as possible in the exhaust ducting. The intention was to minimize the effect of the flow unsteadiness and to insure adequate mixing of the exhaust products. The effect of the unsteadiness was minimized by averaging over a 30 s window when the rig had reached thermal steady state, as well as by translating the probe across the exhaust duct in order to confirm that the spatial variation was minimal.

4. Combustor Exit Gas Temperature Based on CO_2 Concentration

The sample from the same emissions probe was also diverted to a California Analytical CO_2 Model 603 NDIR gas analyzer that was also calibrated and normally used in the GEGR combustion test cells. As with the O_2 concentration, the combustor exit gas temperature was back-calculated using an equilibrium calculation based on the CO_2 concentration.

5. Temperature Based on Power and Measured Downstream Temperature

The turbine inlet temperature (T_4) was also estimated by rearranging the equation for the turbine power as follows:

$$\dot{W}_t = \dot{m}(h_4 - h_5) = \dot{m}C_{pT4}(T_4 - T_5)$$
$$\Rightarrow T_4 = \frac{\dot{W}_{t_{\text{indirect}}} + \dot{m}C_{pT4}T_5}{\dot{m}C_{pT4}} \quad (5)$$

where $W_{t_{\text{indirect}}}$ is the indirect turbine power, m is the mass flow rate through the turbine, C_{pT4} is the specific heat for the combustion products of ethylene-air and T_5 is the measured turbine exit temperature.

6. Combustor Exit Gas Temperature Based on Equivalence Ratio with UHC Corrections

The combustor exit gas temperature was calculated assuming constant pressure equilibrium combustion of the ethylene-air reactant mixture of known equivalence ratio, as determined by the measured total air and fuel mass flow rates. The primary and secondary air mass flow rates were calculated using ASME standard orifice plates in the upstream facility piping. The total air mass flow rate through the turbine was then taken to be the sum of these two quantities. The fuel mass flow rate was measured using a calibrated venturi and the amount of fuel burned was determined by correcting for UHC measured using a California Analytical Model 300 HFID emissions analyzer. The percent UHC was determined by first flowing fuel through the rig (without igniting the spark) at exactly the same operating conditions (inlet mass flows, pressures, temperatures) and pulse-detonation-combustor timing diagram (fuel valve timing). This UHC value represented the baseline zero percent burned count. The rig was then immediately run in PDC-fired mode and the UHC recorded provided the unburned count. The percentage of unburned fuel was determined using

$$\%\text{Unburned Fuel} = \frac{\text{UHC Count During PDC Fired}}{\text{UHC Count [No Ignition]}} \quad (6)$$

The UHC data was used to correct the fuel mass flow rate to provide an estimate for the amount of fuel actually burned using the following equation:

$$\Phi_{\text{corrected}} = (1 - \%\text{Unburned Fuel})\Phi_{\text{baseline}} \quad (7)$$

where $\Phi_{\text{corrected}}$ is the corrected equivalence ratio (representing the amount of fuel actually burned), % unburned fuel is defined preceding and Φ_{baseline} is the equivalence ratio calculated from the air and fuel venturi mass flow rates. The corrected equivalence ratio was then used to estimate the combustor exit gas temperature using an equilibrium combustion calculation. Evidence of UHCs in similar single tube PDE rigs were reported by Klingbeil et al. [24]. The UHCs were the result of a design flaw that was discovered during operation of the rig. Further investigation revealed that the detailed design of the fuel injection was such that the backpressure from the detonation wave trapped some of the fuel in the injector. As result, this trapped fuel subsequently entered the PDC during the purge phase when the tube pressure had dropped sufficiently.

7. Summary Turbine Inlet Temperature Measurements

Figure 7 shows a summary comparison of the turbine inlet temperature measurement using each of the preceding six techniques for a representative run of each type (*eg.*, PDE TIP steady, PDE TIP steady burner, PDC-fired). The PDE TIP steady data had very good agreement with the three methods available (no fuel was combusted, so emissions-based techniques were not applicable). The steady burner also had good agreement between four of the methods, with the exception being the actual thermocouple measurements, which were significantly higher. For the PDC-fired operation, four methods agreed fairly well, with the O_2 and CO_2 concentration-based combustor exit gas temperatures measuring significantly higher. These trends were typical for each type of run, respectively. The standard error on the mean for each data set was approximately ± 50°F, further supporting this value as the measurement uncertainty. Based on this data, it was decided that the final turbine inlet temperature used for the performance calculations was the average of all the methods applicable for a given run. All data presented in this section used this turbine inlet temperature.

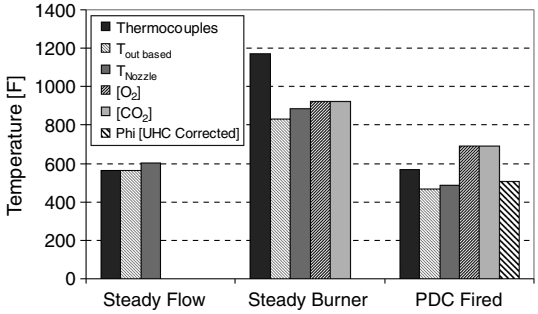

Fig. 7 Comparison of turbine inlet temperature methods.

B. Turbine Performance

1. Steady Air Flow Results

To baseline the PDC-turbine hybrid rig with known existing turbine maps, the rig was operated with heated, nonvitiated steady flow at selected design points. The tests were performed by flowing heated air through the PDC tubes (primary air) and room temperature air through the coaxial cooling passage (secondary air). A primary concern was the effect of the pattern factor on turbine operation. Under normal turbocharger operation, the heated air is directed into the turbine through a full annulus with relatively spatially uniform temperature and pressure (i.e., small pattern and form factor). The more uniform flow would allow for better turbine performance and would also allow for easier measurement of the turbine inlet temperature. Baselining the PDC-turbine hybrid with steady heated air through the can-annular multitube PDC (as opposed to the diffuser inlet used with normal turbocharger operation) allowed an evaluation of the performance of the turbine with the pattern factor due to the multitube PDCs.

Figure 8 shows the performance maps for the steady air flow data points measured with the PDC-turbine hybrid configuration compared with prior results obtained during normal turbocharger operation. The uncertainty bar shown in the top left of each graph was computed by propagation of uncertainty analysis and includes the uncertainty on temperature, pressure and other relevant quantities. Figure 8a shows constant corrected speed lines of normalized power ($\Delta h/T$) versus turbine pressure ratio for the present turbine as computed using a quasi-one-dimensional turbine design tool. The Turbo Steady data refers to the operation of the turbocharger in its native installed configuration, whereas the PDE TIP Steady data refers to operation of the installed PDC-turbine hybrid rig under steady nonvitiated flow. It can be seen that the turbine performance was indistinguishable between these installed geometries (i.e., the turbine performance did not degrade with the can-annular multitube PDC installed upstream). Note that attempts were made to maintain reasonably similar corrected speeds (indicated in square brackets in the legend) in order to make valid comparisons. This provided confidence in the turbine inlet temperature measurement technique and also seemed to suggest that pattern factor was not a strong influence for the performance of this particular turbine. Figure 8b shows similar results for the turbine efficiency as a function of pressure ratio, with similarly good agreement for both the corrected speeds. There is one data point that seems lower than the others, but it is within the uncertainty of ± 8 points. To clarify the definition of "point", a 5-point improvement would represent improving the turbine isentropic efficiency from, for example, 80 to 85%, or 88 to 93%.

2. Steady-Burner Results

The multitube PDC-turbine hybrid rig was operated in a steady-burner mode (during the second test cell entry) to evaluate the turbine performance and measurement techniques when operating with

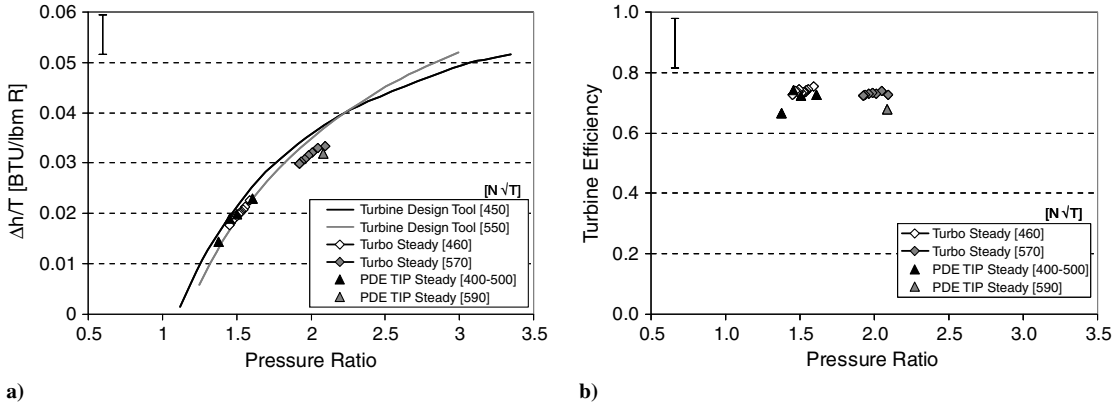

a) b)

Fig. 8 Performance data for PDE TIP steady flow.

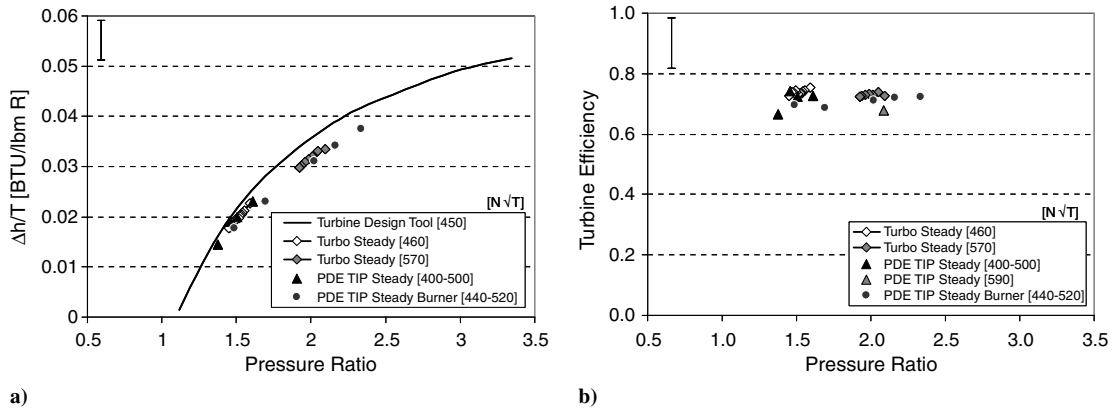

a) b)

Fig. 9 Performance data for PDE TIP steady-burner configuration.

vitiated air. In addition, this data provided a comparison baseline for steady combustion performance versus unsteady combustion (PDC-fired) performance. The intention was to better match the gas properties (C_p and γ) for the turbine flow in order to make a more valid comparison. For the steady-burner configuration, the fuel-air mixing element used in PDC operations was directly interchanged with a fuel-air steady burner designed specifically for this test. In addition, the DDT geometry was removed from the PDC. No other modifications were made to the rig.

Figure 9 compares the steady-burner test points with the performance map. The steady-burner data ranges from corrected speed of 440 to 520 and is compared with the turbine design tool line for corrected speed of 450. The steady-burner data is found to be consistently lower than the turbine design tool analysis (likely due to the imperfect comparison since corrected speeds are slightly different). It does, however, generally follow the correct shape of the curve and, more importantly, is consistent with the previously measured steady-flow data from production hardware.

3. *PDC-Fired Results*

The multitube PDC-turbine hybrid rig was operated in unsteady PDC-fired mode and compared with the steady operation results. As a reminder, PDC-fired operation was achieved using nominally stoichiometric 100% fill of C_2H_4-air mixtures with each tube firing at 20 Hz. For each data point, the rig was first brought up to the desired steady cold air flow condition. Once nominal operation of the turbine was verified, the PDCs were turned on and operated for approximately 5 min (or more) until thermal steady state was achieved. Figure 10 shows a time history of a typical run. The PDCs are turned on at 100 s and the turbine is seen to spool-up to a new speed within about 30 s. Performance data was taken by averaging within the 30 s window (vertical dashed lines) after 300 s of operation.

Figure 11a shows all the performance data obtained under PDC-fired operation at nominally 75 kW (100 hp) and corrected speed [i.e., N/sqrt (T_4)] of approximately 350. The data is seen to fall almost exactly on top of the turbine design tool performance curve and the PDE TIP steady-flow data. Furthermore, the data is repeatable as shown by the gray squares, which were obtained during the second test entry, almost one full year after the first entry. It should be noted that it was not possible to obtain steady-burner data at this condition since the burners flamed out at these lower operating conditions. Figure 11b shows the turbine efficiency, which is more difficult to benchmark from the present data. The closest turbo steady-flow data available is for a corrected speed of 460 (open diamonds) showing a turbine efficiency that is approximately eight points higher than the PDE TIP steady-flow data (black triangle). The PDE TIP fired data from the first test cell entry appears to have a slightly higher efficiency, whereas the PDE TIP fired data from the second test cell

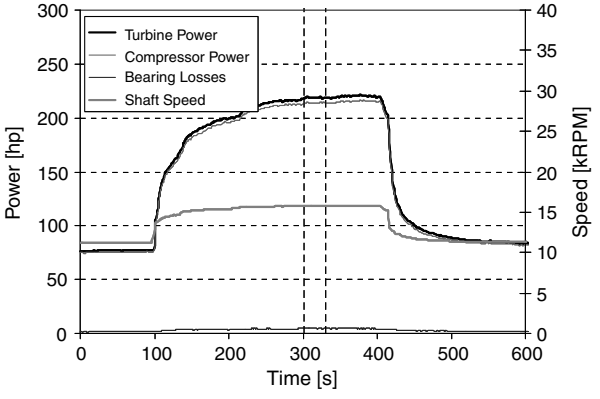

Fig. 10 Measured power time history of a typical PDC-fired run.

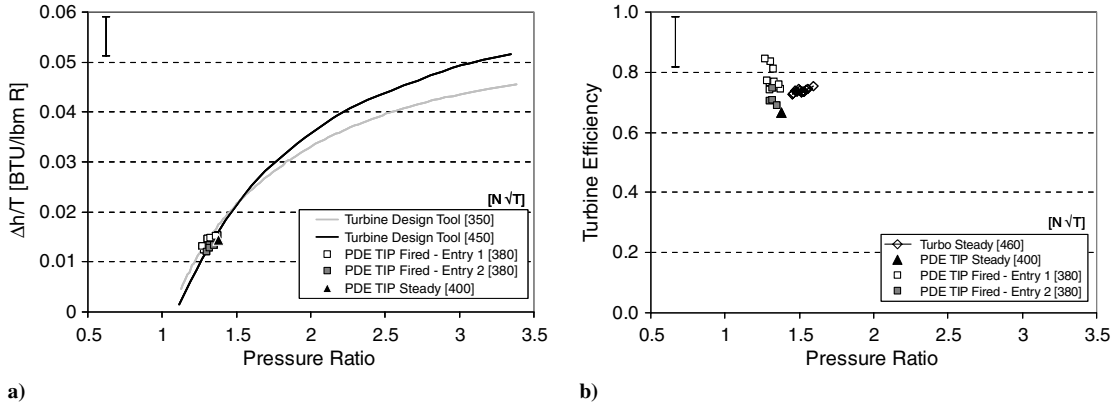

Fig. 11 Performance data for PDC-fired operation at nominal 75 kW (100 hp) condition.

entry appears to have a slightly lower efficiency. On average, the PDC-fired efficiency is about the same as the as the turbo steady-flow efficiency. All the data falls within the uncertainty of ±8 points and it is not possible to distinguish between the results from the present measurements.

Figure 12a shows the normalized power under PDC-fired operation at nominally 150 kW (200 hp) and corrected speed of approximately 460. The PDC-fired data is found to fall slightly below the turbo steady and PDE TIP steady data, however, it is consistent with the PDE TIP steady-burner data. Similar observations are made for the turbine efficiency shown in Fig. 12b. A likely explanation arises from the fact that this data was obtained with only 7 tubes firing since there was a malfunction in one of the tubes. In particular, the water-cooled DDT geometry sprung a leak and was leaking water into the turbine. Since there was limited test time available (not enough to repair the leak), it was decided to continue the experiments with only seven tubes. The offending tube was taken out of commission by shutting off its supply of fuel, spark and DDT cooling water. The primary air, however, was still flowing through the PDC. The turbine, therefore, was experiencing a significant cold spot on a one-eighth sector resulting in an obvious loss of turbine efficiency. The uncertainty bar shown in the top left of each graph was computed by propagation of uncertainty analysis and includes the uncertainty on temperature, pressure and other relevant quantities.

Figures 13a and 13b present summary plots where the multiple PDC-fired data points have been averaged for each of the corrected speed conditions. The uncertainty bars represent the standard error on the mean assuming a 95% confidence interval using a *t*-distribution. The gray hatched region on the turbine efficiency plot shows the overall uncertainty band for the turbine efficiency measurement. As described earlier, the data for the turbo steady, PDE TIP steady, PDE TIP steady-burner and PDC-fired at each condition

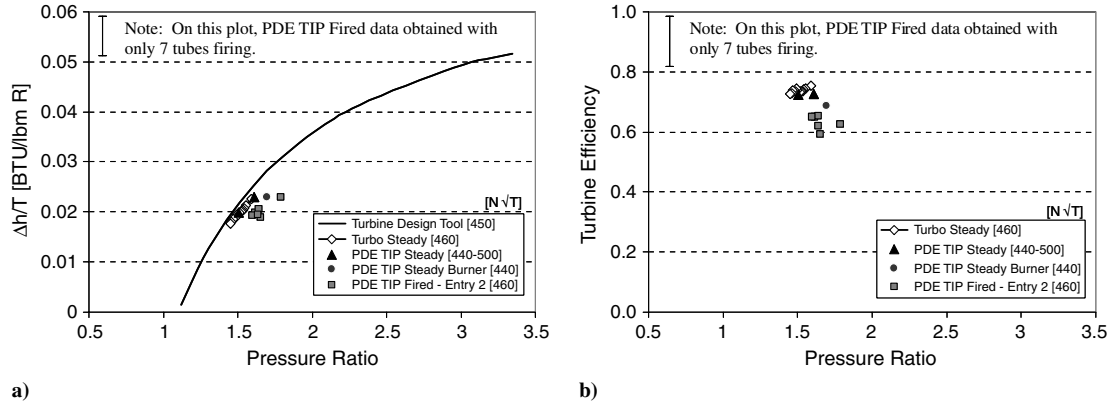

Fig. 12 Performance data for PDC-fired operation at nominal 150 kW (200 hp) condition.

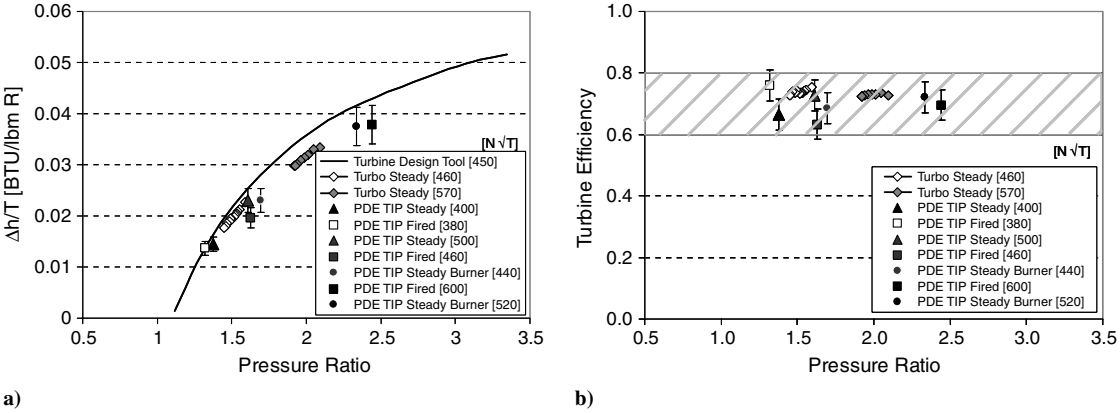

Fig. 13 Summary performance data.

essentially overlap and no distinction in performance was observed with the present instrumentation. These plots also show a comparison between the PDE TIP steady-burner and PDC-fired operation at the highest power of 560 kW (750 hp) that was achieved during the experiments (two right-most data points with normalized power just under 0.04). The agreement is excellent, however, it should be noted that the rig had not reached a thermal steady state when this data was taken (approximately 1 min into the run) since the experiment was shut down due to over temperature conditions at the turbine inlet. The turbine had attained a significant fraction of its estimated steady-state speed (i.e., it was not accelerating as much) and the contribution of its rotational inertia is assumed to be negligible.

4. *Effect of Different Firing Patterns*

Although not explicitly mentioned previously, the test entry 1 data (white squares in Fig. 11) represent the best data set to examine the effect of firing pattern since each data point represents a particular firing pattern. The data was collected within the same hour on the first test entry without modifying any of the facility valve settings and represents the most operationally consistent data. From this data, it can be seen that there was no observed difference in performance using the existing measurement instrumentation. This is likely due to the large measurement uncertainty rather than a true trend since the high-frequency pressure transducer data in Rasheed et al. [27] strongly suggested benefits to different firing patterns. In addition, it should be noted that there were clear differences in the perception of how smooth the rig operated based on the sound of the rig. The sequential firing pattern sounded the "choppiest" and, using high-frequency pressure measurements, this was shown to correspond to tubes misfiring due to tube-to-tube gas dynamic interactions [40] (eg. detonations from one tube diffracting and traveling upstream an adjacent tube, thereby disrupting its proper fill sequence). By contrast, the simultaneous firing pattern sounded the smoothest, and was shown to have the most consistent detonations as measured by high-frequency pressure sensors [40]. Although the simultaneous firing pattern sounded better, it had a tendency to overpressure the primary plenum and rupture the burst disk. This suggests that there were large-scale transient overpressures associated with the simultaneous firing pattern; something that makes sense since the rig would experience one large pressure pulse associated with the simultaneous firing of all the tubes, followed by a long period of lower pressures during the simultaneous blowdown of all the tubes, followed by another large pressure pulse at the beginning of the next cycle. Such large oscillations are typically associated with flow losses, yet the existing performance instrumentation did not have the resolution to observe any differences.

C. Overall Efficiency

In addition to the component level turbine efficiency, an analysis was performed to estimate the overall rig efficiency, which can be defined as follows:

$$\eta = \frac{\text{Output Power}}{\text{Input Power}} = \frac{\text{Indirect Turbine Power}}{\text{Compressor Input} + \text{Heat Input}} = \frac{\dot{W}_t}{\dot{W}_c + \dot{Q}_{\text{in}}} \tag{8}$$

Note that this overall efficiency should not be interpreted as a thermodynamic efficiency since a complete thermodynamic cycle was not represented by the present experimental rig, which only consisted of the combustor and turbine (eg. the heat addition and expansion processes). Rather, the preceding equation is simply used as a means of performing a relative comparison between PDC-fired operation and steady operation. In this equation, W_t is the indirect turbine power as described in detail in the previous section. W_c is the external facility compressor work input (assuming 80% efficiency) required to bring the inlet air from air standard conditions (70°F) to the temperature measured just upstream of the air piping control valve to the rig during the run. This should not be confused with the turbocharger compressor work, which is used as the load for the present experiments. The remaining term, the heat input, was estimated using two different techniques. The first technique used the first law across the PDC tube to estimate the heat input as

$$\dot{Q}_{\text{in1}} = \dot{m}h_{\text{out}} - \dot{m}h_{\text{in}} = \dot{m}C_{p2}T_{\text{out}} - \dot{m}C_{p1}T_{\text{in}} \tag{9}$$

where m was the turbine air flow rate, T_{in} was the mass-averaged temperature from the primary and secondary plenums, C_{p1} was the specific heat of air evaluated at the T_{in}, T_{out} was the measured turbine inlet temperature and C_{p2} was the estimated specific heat of the gas at the combustor exit (or turbine inlet). As before, C_{p2} was estimated by using an equilibrium combustion code to determine the gas properties where the calculated combustor exit gas temperature matched the measured turbine inlet temperature. Once again, this approach provided gas properties representative of the mass-averaged working fluid including all primary and secondary flows.

The second technique used the energy content of the fuel to estimate the heat input:

$$\dot{Q}_{\text{in2}} = \dot{m}_{f_{\text{burned}}}\text{LHV} \tag{10}$$

where $m_{f_{\text{burned}}}$ was the mass flow rate of fuel burned and LHV was the lower heating value of 20, 327 BTU/lbm for ethylene. For a given run, the fuel venturi provided a measurement of the total fuel flow into the rig, which was verified by weighing the fuel bottles before and after a run, and comparing with the cumulative fuel flow as measured by the fuel venturi. The mass flow rate of fuel burned was then estimated by correcting the fuel venturi mass flow rate using the gas sampled UHC measurements. The two techniques of estimating heat input were found to be within 20% of each other for all the runs, and the average value was used in the overall efficiency calculation.

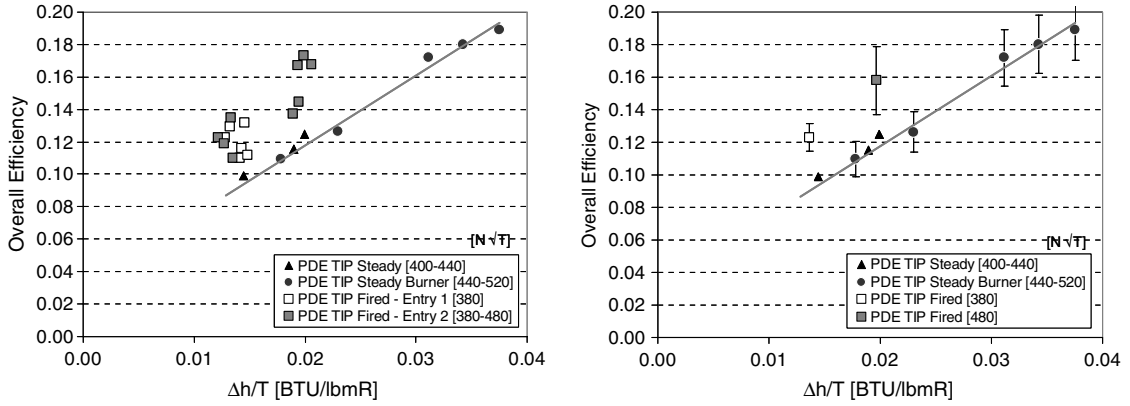

Fig. 14 Overall efficiency for a) all the data and b) summary data.

Figure 14a shows the overall rig efficiency for the steady-flow, steady-burner, and PDC-fired operation as a function of the normalized power. The steady-burner data falls approximately on a straight line and a linear curve fit is shown to help guide the eye. The steady-flow data is seen to match this line very well. It should be noted that the steady flow was nonvitiated and did not have any heat release within the rig (i.e., $Q_{\text{in}} = 0$). The denominator in the calculation was entirely due to the facility compressor work term (W_c), which captured the amount of energy required to bring the inlet air to the steady-flow temperature and pressure. As seen with the turbine performance data, the PDC-fired data falls into two groups representing the low and higher power operating conditions with some scatter. As before, there is excellent agreement between the data taken from the first and second test cell entries, indicating that the data was repeatable. In all cases, the PDC-fired operation is seen to be above the steady-burner operating line suggesting a slight performance benefit. Figure 14b is a summary plot where the PDC-fired data is averaged for the two groups and error bars are shown representing the standard error on the mean with a 95% confidence interval using a *t*-distribution since the number of samples is less than 30. The steady-burner data points are single runs with an estimated uncertainty of ± 2 points. This plot suggests that the rig demonstrated an efficiency benefit of four points (approximately 25%) when operating under PDC-fired operation.

D. Discussion

The present results, which show no measurable adverse impact to turbine efficiency, as well as a potential four-point improvement on rig overall efficiency, are encouraging because no attempts were made to optimize the performance of the PDC-turbine hybrid system. As such, the present rig does not represent the maximum benefit achievable in a PDC-turbine hybrid engine and a number of modifications could be made to further improve the performance of the present rig. The first is to modify the PDC tubes to have an air-valve to provide a closed head end during the detonation and blowdown. The present unvalved configuration allows pressure-waves to travel upstream into the air-inlet system, reducing the effective net pressure-rise that could potentially be achieved [27]. The second would be to improve the fuel injection design so that the fuel is injected at the proper time during the PDE cycle and has a higher combustion efficiency. The third is to directly couple the exit of the PDC tubes to the turbine rotor, thereby eliminating the dump plenum in the present rig, as well as the traditional stator row in gas turbines. The fourth, which is probably the most challenging, would be to design a turbine specifically for PDC flows. Such a turbine might look completely different from existing turbine designs and might require a completely new paradigm. The present rig used an off-the-shelf turbine optimized for steady flow. As such, there was no expectation of improving turbine component efficiency. In fact, the turbine was expected to have, at best, equivalent efficiency under the unsteady PDC-fired operation. The finding that the turbine efficiency did not suffer a measurable degradation in performance is quite promising and suggests that it is possible to develop an optimized turbine geometry. Regardless, it is important to recognize that the system level metric of overall rig efficiency is the more relevant metric when evaluating the benefit of a PDC-turbine hybrid because it highlights the performance advantage of the PDC when compared with a conventional combustor. In particular, for a commercial PDC-turbine hybrid engine, the turbine component efficiency might be lower than typical present-day turbine efficiency designed for steady flow. An overall efficiency benefit will be realized, however, if the performance benefit from the pressure-rise combustion overcomes the lower the turbine efficiency and other unsteady losses. The present experiments represented one of the first experimental efforts to investigate performance of a multitube PDC-turbine hybrid engine configuration. The results are promising since they suggest that the performance benefit of a PDC-turbine hybrid engine could be realized with further development, with a particular emphasis on additional testing to extend the present results to actual engine pressures found in modern gas-turbine engines.

V. Conclusions

The turbine performance (normalized power and turbine efficiency) and overall rig performance were measured by performing 5+ minute runs to allow the PDC-turbine hybrid rig attain thermal steady state. A large amount of data was obtained at two operating conditions under turbo steady-flow, PDE TIP steady-flow, PDE TIP steady-burner and PDC-fired operation. The turbine component efficiency was indistinguishable under steady and PDC-fired operation with the present measurement resolution. This is a particularly encouraging result considering that this rig was not optimized for turbine performance. In addition, the overall rig efficiency was measured and found to show a benefit for PDC-fired operation versus steady combustion. These results are very encouraging and further work is recommended using a rig specifically designed for performance measurements.

Acknowledgments

This work was performed as part of a collaborative effort between the General Electric (GE) Pulse Detonation Advanced Technology Program at the GE Global Research Center (GEGR) and the NASA Constant Volume Combustion Cycle Engine program administered by the NASA-Glenn Research Center (Leo Burkardt, Program Manager). The authors recognize the technical input from Clay Haubert, Venkat Tangirala, Mark Baptista and Jonathan Janssen, as well as the technical support from Eric Cornell and Tony Brand. The hard work of Walt Chandler at GEGR is noteworthy for his role as the primary technician for all assembly, installation and testing for the entire present experimental effort, as well for his technical expertise and experience.

References

[1] Nicholls, J. A., Wilkinson, H. R., and Morrison, R. B., "Intermittent Detonation as a Thrust Producing Mechanism," *Jet Propulsion*, Vol. 27, No. 5, 1957, pp. 534–541.

[2] Roy, G. D., Frolov, S. M., Borisov, A. A., and Netzer, D. W., "Pulse Detonation Propulsion: Challenges, and Current Status," *Progress in Energy and Combustion Science*, Vol. 30, No. 6, 2004, p. 545. doi:10.1016/j.pecs.2004.05.001

[3] Kailasanath, K., "Recent Developments in Research on Pulse Detonation Engines," *AIAA Journal*, Vol. 41, No. 2, 2003, pp. 145–159. doi:10.2514/2.1933

[4] Powers, J., and Frolov, S. M., "Perspectives on Detonation-Based Propulsion," *Journal of Propulsion and Power*, Vol. 22, No. 6, 2006, pp. 1153–1154. doi:10.2514/1.26953

[5] Fickett, W., and Davis, W. C., *Detonation: Theory and Experiment*, Dover, Mineola, NY, 2000.

[6] Wintenberger, E., Austin, J., Cooper, M., Jackson, S., and Shepherd, J., "Analytical Model for the Impulse of Single-Cycle Pulse Detonation Tube," *Journal of Propulsion and Power*, Vol. 19, No. 1, 2003, pp. 22–38. doi:10.2514/2.6099

[7] Wintenberger, E., and Shepherd, J., "Model for the Performance of Airbreathing Pulse-Detonation Engines," *Journal of Propulsion and Power*, Vol. 22, No. 3, 2006, pp. 593–602. doi:10.2514/1.5792

[8] Ma, F., Choi, J.-Y., and Yang, V., "Propulsive Performance of Airbreathing Pulse Detonation Engines," *Journal of Propulsion and Power*, Vol. 22, No. 6, 2006, pp. 1188–1203. doi:10.2514/1.21755

[9] Harris, P. G., Stowe, R. A., Ripley, R. C., and Guzik, S. M., "Pulse Detonation Engine as a Ramjet Replacement," *Journal of Propulsion and Power*, Vol. 22, No. 2, 2006, pp. 462–473. doi:10.2514/1.15414

[10] Heiser, W. H., and Pratt, D. T., "Thermodynamic Cycle Analysis of Pulse Detonation Engines," *Journal of Propulsion and Power*, Vol. 18, No. 1, Jan.–Feb. 2002, pp. 68–76. doi:10.2514/2.5899

[11] Kentfield, J. A. C., "Thermodynamics of Airbreathing Pulse-Detonation Engines," *Journal of Propulsion and Power*, Vol. 18, No. 6, 2002, pp. 1170–1175. doi:10.2514/2.6075

[12] Goldmeer, J., Tangirala, V. E., and Dean, A. J., "System-Level Performance Estimation of a Pulse Detonation Based Hybrid Engine," *Journal of Engineering for Gas Turbines and Power*, Vol. 130, No. 1, Jan. 2008, p. 011201. doi:10.1115/1.2771246

[13] Allgood, D. C., Gutmark, E., Hoke, J., Bradley, R., and Schauer, F., "Performance Measurements of Multicycle Pulse-Detonation-Engine Exhaust Nozzles," *Journal of Propulsion and Power*, Vol. 22, No. 1, 2006, pp. 70–77.

[14] Owens, Z. C., and Hanson, R. K., "Single-Cycle Unsteady Nozzle Phenomena in Pulse Detonation Engines," *Journal of Propulsion and Power*, Vol. 23, No. 2, March–April 2007, pp. 325–337. doi:10.2514/1.22415

[15] Cooper, M., and Shepherd, J. E., "Single-Cycle Impulse from Detonation Tubes with Nozzles," *Journal of Propulsion and Power*, Vol. 24, No. 1, 2008, pp. 81–87. doi:10.2514/1.30192

[16] Wilson, J., Sgondea, A., Paxson, D., and Rosenthal, B., "Parametric Investigation of Thrust Augmentation by Ejectors on a Pulse Detonation Tube," *Journal of Propulsion and Power*, Vol. 23, No. 1, 2007, pp. 108–115. doi:10.2514/1.19670

[17] Allgood, D. C., Gutmark, E., Rasheed, A., and Dean, A. J., "Experimental Investigation of a Pulse Detonation Engine with a Two-Dimensional Ejector," *AIAA Journal*, Vol. 43, No. 2, 2005, pp. 390–398. doi:10.2514/1.8125

[18] Glaser, A. J., Caldwell, N., Gutmark, E., Hoke, J., Bradley, R., and Schauer, F., "A Study on the Operation of Pulse Detonation Engine Driven Ejectors," *Journal of Propulsion and Power*, Vol. 24, No. 6, 2008, pp. 1324–1331. doi:10.2514/1.37869

[19] Kailasnath, K., "Liquid-Fueled Detonations in Tubes," *Journal of Propulsion and Power*, Vol. 22, No. 6, 2006, pp. 1261–1268. doi:10.2514/1.19624

[20] Frolov, S. M., "Liquid-Fueled, Air-Breathing Pulse Detonation Engine Demonstrator: Operation Principles and Performance," *Journal of Propulsion and Power*, Vol. 22, No. 6, 2006, pp. 1162–1169. doi:10.2514/1.17968

[21] Jian-Zhong, L., "Investigation on Common Nozzle of Triple-Tube Pulse Detonation Engine with Kerosene/Air," *Journal of Aerospace Power*, Vol. 23, No. 5, May 2008, pp. 840–844 (in Chinese).

[22] Cooper, M., and Shepherd, J. E., "Detonation Tube Impulse in Subatmospheric Environments," *Journal of Propulsion and Power*, Vol. 22, No. 4, 2006, pp. 845–851. doi:10.2514/1.16979

[23] Mattison, D. W., Brophy, C. M., Sanders, S. T., Ma, L., Hinckley, K. M., Jeffries, J. B., and Hanson, R. K., "Pulse Detonation Engine Characterization and Control Using Tunable Diode-Laser Sensors," *Journal of Propulsion and Power*, Vol. 19, No. 4, 2003, pp. 568–572. doi:10.2514/2.6167

[24] Klingbeil, A. E., Jeffries, J. B., and Hanson, R. K., "Design of a Fiber-Coupled Mid-Infrared Fuel Sensor for Pulse Detonation Engines," *AIAA Journal*, Vol. 45, No. 4, 2007, pp. 772–778. doi:10.2514/1.26504

[25] Schauer, F., Stutrud, J., Bradley, R., Katta, V., and Hoke, J., "Detonation Studies and Performance Results for a Research Pulse Detonation Engine," *Confined Detonations and Pulse Detonation Engines*, edited by G. Roy, S. Frolov, R. Santoro, and S. Tsyganov, Torus, Moscow, 2003, pp. 275–290.

[26] Glaser, A., Rasheed, A., Dunton, R., and Tangirala, V. E., "Investigations of Thrust Generated by a Valved, Multi-Tube PDE with Exit Nozzles," 44th AIAA/ASME/SAE/ASEE Joint Propulsion Conference, Hartford, CT, AIAA Paper 2008-4692, 21–23 July 2008.

[27] Rasheed, A., Furman, A. H., and Dean, A. J., "Experimental Investigations of an Axial Turbine Driven by a Multi-Tube Pulsed Detonation Combustor System," 41st AIAA/ASME/SAE/ASEE Joint Propulsion Conference, Tucson, AZ, AIAA Paper 2005-4209, 10–13 July 2005.

[28] Petters, D. P., and Felder, J. L., "Engine System Performance of Pulse Detonation Concepts Using the NPSS Program," AIAA Paper 2002-3910, 2002.

[29] Tangirala, V. E., Rasheed, A., and Dean, A. J., "Performance of a Pulse Detonation Combustor-Based Hybrid Engine," ASME Turbo Expo 2007, Montreal, International Gas-Turbine Institute Paper GT2007-28056, 14–17 May 2007.

[30] Tangirala, V. E., and Joshi, N. D., "Systems Level Performance Estimations for a Pulse Detonation Combustor Based Hybrid Engine," ASME Turbo Expo 2008, Berlin, International Gas-Turbine Institute Paper GT2008-51525, 2008.

[31] Endo, T., "Thermodynamic Analysis of the Performance of a Pulse Detonation Turbine Engine," *Science and Technology of Energetic Materials*, Vol. 65, No. 4, 2004, pp. 103–110 (in Japanese).

[32] Deng, J., Chuanjun, Y., Zheng, L., Qiu, H., and Jiang, L., "Calculating Performance of Gas Turbine Engine with Embedded PDC," *Journal of Northwestern Polytechnical University*, Vol. 26, No. 3, June 2008, pp. 362–367 (in Chinese).

[33] Hoke, J., Royce, B., Stutrud, J., and Schauer, F., "Integration of a Pulsed Detonation Engine with an Ejector Pump and with a Turbo-Charger as Methods to Self-Aspirate," 40th AIAA Aerospace Sciences Meeting and Exhibit, Reno, NV, AIAA Paper 2002-0615, 2002.

[34] Schauer, F., Bradley, R., and Hoke, J., "Interaction of Pulsed Detonation Engine With a Turbine," 41st AIAA Aerospace Sciences Meeting and Exhibit, Reno, NV, AIAA Paper 2003-0891, 6–9 Jan. 2003.

[35] Dean, A. J., Rasheed, A., Tangirala, V. E., and Pinard, P. F., "Operation and Noise Transmission of an Axial Turbine Driven by a Pulse Detonation Combustor,"*Proceedings of International Gas-Turbine Institute*; also American Society of Mechanical Engineers Paper GT-2005-69141, 6–9 June 2005.

[36] Glaser, A., Caldwell, N., and Gutmark, E., "Performance Measurements of a Pulse Detonation Combustor Array Integrated with an Axial Flow Turbine," 44th AIAA Aerospace Sciences Meeting and Exhibit, Reno, NV, AIAA Paper 2006-1232, 9–12 Jan. 2006.

[37] Glaser, A., Caldwell, N., and Gutmark, E., "Performance of an Axial Flow Turbine Driven by Multiple Pulse Detonation Combustors," 45th AIAA Aerospace Sciences Meeting and Exhibit, Reno, NV, AIAA Paper 2007-1244, 8–11 Jan. 2007.

[38] Caldwell, N., Glaser, A., and Gutmark, E., "Performance Measurements of a Pulse Detonation Engine Array with a Turbine," 42nd AIAA/ASME/SAE/ASEE Joint Propulsion Conference and Exhibit, Sacramento, CA, AIAA Paper 2006-4307, 9–12 July 2006.

[39] Caldwell, N., Brunet, R., Gutmark, E., and Drouin, B., "Experimental Analysis of a Hybrid Pulse Detonation Combustor/Gas Turbine Engine," 46th AIAA Aerospace Sciences Meeting and Exhibit, Reno, NV, AIAA Paper 2008-0121, 7–10 Jan. 2008.

[40] Rasheed, A., Furman, A. H., and Dean, A. J., "Pressure Measurements and Attenuation in a Hybrid Multi-Tube Pulse Detonation System," *Journal of Propulsion and Power*, Vol. 25, No. 1, Jan.–Feb. 2009, pp. 148–161. doi:10.2514/1.31893

J. Powers
Associate Editor